Catal Surv Asia (2009) 13:30–40
DOI 10.1007/s10563-009-9065-9

Photocatalytic Reduction of Greenhouse Gas CO_2 to Fuel

Jeffrey C. S. Wu

Published online: 26 February 2009

Abstract Sun is the Earth's ultimate and inexhaustible energy source. One of the best routes to remedy the CO_2 problem is to convert it to valuable hydrocarbons using solar energy. In this study, CO_2 was photocatalytically reduced to produce methanol, methane and ethylene in a steady-state optical-fiber reactor under artificial light and real sunlight irradiation. The photocatalyst was dip-coated on the optical fibers that enable the light to transmit and spread uniformly inside the reactor. The optical-fiber photoreactor, comprised of nearly 120 photocatalyst-coated fibers, was designed and assembled. The XRD spectra indicated the anatase phase for all photocatalysts. It is found that the methanol yield increased with UV light intensity. A maximum methanol yield of 4.12 μmole/g-cat h is obtained when 1.0 wt% Ag/TiO_2 photocatalyst was used under a light intensity of 10 W/cm^2. When mixed oxide, TiO_2–SiO_2, is doped with Cu and Fe metals, the resulting photocatalysts show substantial difference in hydrocarbon production as well as product selectivity. Methane and ethylene were produced on Cu–Fe loaded TiO_2–SiO_2 photocatalyst. Since dye-sensitized Cu–Fe/P25 photocatalyst can fully harvest the light energy of 400–800 nm from sunlight, its photoactivity was significantly enhanced. Finally, CO_2 photoreduction was studied by in situ IR spectroscopy and possible mechanism for the photoreaction was proposed.

Keywords Photocatalysis · Renewable energy · Optical-fiber photoreactor · CO_2 photoreduction · TiO_2 · Dye-sensitization

J. C. S. Wu (✉)
Department of Chemical Engineering, National Taiwan University, Taipei, Taiwan 10617, ROC
e-mail: cswu@ntu.edu.tw

1 Introduction

Greenhouse gases such as carbon dioxide (CO_2), methane (CH_4) and chlorofluorocarbons (CFCs) are the primary causes of global warming. Among them, CO_2 is released mainly by the burning of fossil fuels. Over the past decades, the atmospheric concentration of CO_2 has been increasing owing to the expanded human activity, which consequently has accelerated the greenhouse effect. On the other hand, the consumption of fossil fuels worldwide gradually increases year after year because of the strong demand for human activities. Therefore, converting CO_2 to valuable hydrocarbons is one the best solutions to both the global warming and the energy shortage problems.

Figure 1 depicts the energy cycle using carbon as a carrier. Not only all lives make use of the solar energy, but also the fossil fuel is the storage of solar energy via photosynthesis in the past. In nature, CO_2 is removed from the environment by photosynthesis. The energy obtained from sunlight is ultimately used to convert CO_2 into glucose—a sugar molecule that stores sun energy in the form of chemical energy. Except geothermal or nuclear energy, most energy forms, such as fossil fuel, bio-material, hydropower, wind, etc., are simply transformations of sun energy either in the past or present. Thus solar energy is the Earth's ultimate energy supply. One of the promising routes is that artificial photosynthesis may be implemented via the photoreduction of CO_2 to produce hydrocarbons. That is, solar energy is directly transformed and stored as chemical energy. Consequently, the photoreduction of CO_2 to chemicals, such as methane or methanol, is particularly interesting, and achieving a high efficiency for this reaction is extremely desired. Methanol can be easily transported, stored and used as gasoline-additives for automobiles. Moreover, methanol can be transformed into other useful chemicals using conventional chemical technologies.

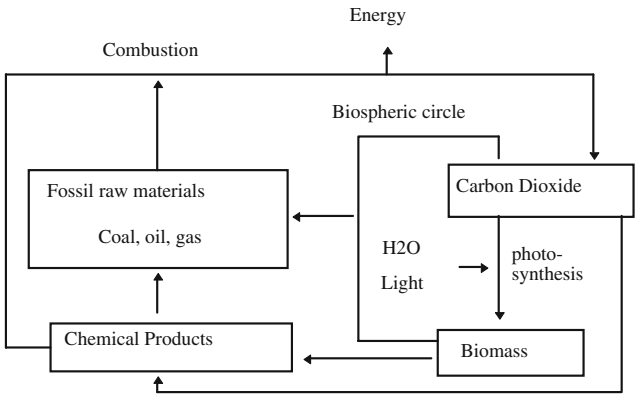

Fig. 1 Energy cycle using carbon as the energy carrier

The energy grade of CO_2 is low from a thermodynamic perspective, which is why any transformation to hydrocarbon requires energy infusion. Equation 1 gives an example of the overall photoreduction of CO_2 to methanol. Based on thermodynamics, converting one mole of CO_2 into methanol requires 228 kJ (ΔH) of energy at 298 K. Furthermore, the Gibbs free energy of Eq. 1 is 698.7 kJ (ΔG) at 298 K indicating that the equilibrium is highly unfavorable to the product, methanol and oxygen. The energy source should be provided without producing more CO_2. Plants use solar energy to perform photosynthesis, but the efficiency of energy transformation is low at the cost of supporting their lives. Even under the optimal artificial conditions, energy efficiency can only reach about 7% in macroalga under full sunlight [1].

$$CO_2 + 2H_2O \xrightarrow{hv} CH_3OH + \frac{3}{2}O_2 \quad (1)$$

Photocatalysis uses semiconductor materials to drive reactions in the presence of light radiation. Semiconductors exhibit a bandgap, which a pair of electron-hole (e^- and h^+) is generated under light radiation. Photocatalytic process occurs via the direct absorption of photons with energy greater than or equal to the bandgap to generate electron-hole pairs. The initial excitation and electron transfer make chemical reactions in the photocatalytic process possible. Many researchers have shown that CO_2 can be reduced in water vapor or solvent by photocatalysts. Titanium oxide catalysts were prepared and utilized as photocatalysts for the reduction of CO_2 with H_2O to produce CH_4 and CH_3OH [2–7]. Recently, Guan et al. [8, 9] reported the photoreduction of CO_2 with H_2O under concentrated sunlight using $K_2Ti_6O_{13}$-based photocatalysts. The selective photoreduction of CO_2 into methanol was studied using ZnO and NiO under UV laser irradiation [10]. NiO/$InTaO_4$, an efficient visible-light photocatalyst, was shown that these catalysts had ability to reduce CO_2 into methanol [11, 12]. Organic sensitizers capable of electron generation under illumination were used to initiate CO_2 photoreduction on TiO_2 thin and thick film surfaces [13–16]. Significantly improved photo conversion of CO_2 was reported using nanoscale TiO_2 particles embedded on silver-coated Nafion membrane film [17]. Ru–TiO_2/SiO_2 was prepared by solid-state dispersion method and used for the photoreduction of carbon dioxide in aqueous medium at ambient conditions [18]. The CO_2 photoreduction of zinc-phthalocyanine-loaded TiO_2 was markedly increased because of the lowering recombination probability for hole-electron pairs [19]. Although various catalysts gave different efficiencies of photo-energy conversion, there is still room to be improved.

Practical applications of photocatalyst for the photoreduction of CO_2 at continuous steady-state often require immobilizing the photocatalyst in a photoreactor. However, traditional packed-bed reactor with light irradiation either from side or center always projects shadow on the other side of photocatalyst particle, which makes part of photocatalyst surface ineffective in a photo-driven reaction. The transmission and uniform distribution of light energy are important in designing a photoreactor that differs completely from a traditional reactor. Hofstadler et al. [20] used titanium dioxide-coated fused-silica glass fibers for wastewater treatment. A single TiO_2-coated fiber-optic reactor was designed by Danion et al. [21]. The TiO_2-coated optical fiber photoreactor was built and further studied in order to optimize different parameters before the development of a multi-optical fiber reactor [22–25]. Peill and Hoffmann demonstrated that TiO_2-coated optical-fiber reactors had some inherent advantages over packed-bed reactors in photoreactions [26–31]. In general, a bundle of optical fibers can provide a very high exposure surface area per unit volume in a photoreactor.

In this research work, an optical-fiber reactor was designed and assembled to exhibit the advantages in photo reactions, especially in the photoreduction of CO_2. The feasibility of sunlight harvest was also demonstrated using concentrated sunlight system.

2 Theoretical Light Transmission in an Optical Fiber

Figure 2 shows that light is transmitted into an optical fiber. The light is split into two beams when hitting the internal fiber surface, due to the difference of refraction index between the TiO_2 coating and the silica core. Part of the light is reflected and transmitted along the fiber, while the rest penetrates and excites the titania layer at the interface. The light gradually spreads and diminishes to the end of the fiber. Upon photo-excitation, the electron-hole (e^- and h^+) pairs are generated on TiO_2 photocatalyst to carry out the subsequent photoreaction. Therefore, optical

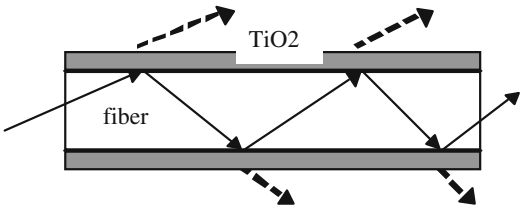

Fig. 2 The schematic of light transmission and spread of TiO_2 coated optical fiber

fiber can be regarded as a medium to deliver light effectively and uniformly to the photocatalyst surface, hence increasing the efficiency of photo-energy conversion in a photoreactor. Beam propagation method (BPM) is used to calculate the transmission loss on an optical fiber [32]. The power loss is due to the absorption of photo-energy by TiO_2 film, which decays exponentially along the optical fiber. Base on this result, it is estimated that the remaining power will decrease to 1% in a 11.4 cm long optical fiber. Therefore, the length of optical fiber should be designed near 11.4 cm so that most photo-energy would be absorbed by the TiO_2 film in a photoreactor.

3 Experimental

3.1 Preparation of TiO_2 Coated Optical Fiber

The TiO_2 solutions to be on optical fibers were prepared by the thermal hydrolysis method. Titanium (IV) butoxide and polyethylene glycol (PEG, molecular weight of 20,000, Merck, Darmstadt, Germany) were added to a 0.1 M nitric acid solution. The volume ratio of titanium butoxide to HNO_3 was 1:6, and the weight of PEG was 50% of that of TiO_2. The appearance of pure TiO_2 solution was milky and slightly transparent. PEG was added to prevent cracking during the drying and calcination of the film. Furthermore, it tends to increase the viscosity of the solution as well as the uniformity TiO_2 particles dispersed in the solution. An appropriate amount of metal precursor, such as $CuCl_2$ or $AgNO_3$, was added to obtain the desired metal loading of TiO_2. The mixed solution was stirred and heated to 80 °C for 8 h. Detailed preparation procedure was reported in literature [33].

Optical fibers were obtained from the E-Tone Technology Company of Taiwan. The polymeric shield on the optical fiber was burned off in a furnace at 400 °C. The remaining quartz fiber had a diameter of 112 μm. Each quartz fiber was cleaned by a 5 M NaOH solution in an ultrasonic cleaner, and then rinsed in de-ionized water and dried before applying dip-coating procedure. The bare fiber was immersed into the solution vertically, and then pulled up at various rates by a step motor. The pulling-up rates ranged from 5 to 50 mm/min. The TiO_2 coated optical fibers were dried in air at 150 °C with a rate of 1 °C/min from the ambient temperature, and maintained at 150 °C for 3 h. Then it was calcined at 500 °C for another 5 h. The TiO_2 film on optical fiber was durable and has passed the "Cross-Cut tape test", according to the methods described in ISO 2409 and ASTM D3359 [34].

Synthesis of TiO_2–SiO_2 mixed oxide was carried out in two steps [35]. The two solutions were mixed and refluxed at 80 °C for 1 h under vigorous stirring (ca. 1,500 rpm). Acetyl acetone (acac, Merck) was employed as a chelating agent. The first solution consisted of corresponding volume of chelating agent in 15 mL of solvent (50% v/v of ethanol and isopropanol). The second one was Tetraisopropoxytitanium (TTIP, Merck) diluted in 35 mL of solvent. The resulted deep-yellow transparent liquid (when the acac as a chelating agent was used) or a colorless transparent liquid (without chelating agent) was cooled to ambient temperature for 1 h. The solution is denoted as modified TTIP.

The hydrolysant (35% hydrochloric acid and the amount of de-ionized water used in 10 mL of solvent) was added to tetraethyl orthosilicate (TEOS, Merck) solution via a dropping funnel and vigorously stirred at 50 °C for 45 min, which is referred to as the pre-hydrolysis of TEOS. After that, the modified TTIP as described above was added into the solution under vigorous stirring. After 10 min, the hydrolysis was completed by addition of the residual amount of de-ionized water diluted in 18 mL of solvent under vigorous stirring. Finally, 15 of mL solvent was introduced after another 10 min had elapsed.

The molar ratio of alkoxides:water:hydrochloric acid: solvents was 1:4:0.19:5 and the content of SiO_2 in TiO_2–SiO_2 mixed oxides was 5 wt%. The sol-gel solution was aged for 24 h at room temperature and then dried in the oven at 80 °C for 24 h. The resulting xerogel was calcined in static air at 500 °C for 2 h.

The molar ratio of 1 for acac/TTIP was employed to prepare TiO_2–SiO_2-acac sample. The sample prepared without using chelating agent was denoted as TiO_2–SiO_2. For the preparation of metal doped TiO_2–SiO_2, the same synthesis procedure for TiO_2–SiO_2 mixed oxide as described above was employed except that the corresponding metal salts were mixed with the derived TiO_2–SiO_2 sol-gels after the sol-gel processes.

Commercial titanium dioxide powder (P25, Degussa) was used as a TiO_2 source to prepare dye-sensitized photocatalysts. $Cu(NO_3)_2 \cdot 3H_2O$ and $Fe(NO_3)_3 \cdot 9H_2O$ (Aldrich) were employed as precursors of metal dopants on P25 support. $Ru^{II}(2,2'\text{-bipyridyl-}4,4'\text{-dicarboxylate})_2\text{-}(NCS)_2$ (also called N3-dye, Solaronix) was used as a dye sensitizer that was dissolved in ethanol (99.5%) to obtain a 3 mM dye solution.

P25 slurry with corresponding metal salts was prepared by adding aqueous PEG solution with the metal salts to P25

powder in a mortar under vigorous grinding with pestle [36]. The prepared uniform lump-free slurry was coated on optical fibers by dip-coating method. Dye-adsorbed photocatalyst was obtained by dipping the corresponding photocatalyst into the 3 mM dye solution for 24 h. Subsequently, dye-adsorbed photocatalyst was rinsed with ethanol (99.5%) to obtain a monolayer of dye on the photocatalyst surface. The resulting dye-adsorbed photocatalyst was finally put in an oven at 80 °C for 30 min to remove the residue solvent on the surface of the photocatalyst.

3.2 Photoreduction of CO_2

An optical-fiber photoreactor (OFPR) was designed and assembled to transmit light to the fiber-supported TiO_2 film from one side of the OFPR module, as shown in Fig. 3. The fibers with length of nearly 11 cm long were inserted into the OFPR. The optical fibers were supported on circular plates with a diameter of 5.0 cm. The OFPR was irradiated by artificial light or concentrated natural sunlight through the quartz window at one side. The artificial light (320–500 nm) was supplied by Exfo Acticure 4,000 with a highest intensity at 365 nm using an appropriate color filter. The light intensity could be tuned and measured with a Lumen meter (Exfo). A solar concentrator (Himawari, Japan) was used to collect natural sunlight. The reflection dish of the solar concentrator is able to track the sun trajectory during a day so that the maximum sunlight intensity can be obtained. The concentrated sunlight is transmitted via an optical cable and focused on the window of the photoreactor. The reactor was wrapped with a heating tape connected to temperature controller with a thermocouple placed at the center of the reactor to maintain the reaction temperature. The reactor was purged by CO_2 gas bubbling through distilled water for 1 h before the reaction. The space velocity of CO_2 gas and H_2O vapor was maintained at nearly 0.72 h^{-1}. The photo reactions were carried out at steady state and lasted for 6–24 h. Some reactions were repeated two or three times, and the deactivation of catalysts was found to be negligible. The outlet gases were analyzed by a GC equipped with FID and porapak Q column.

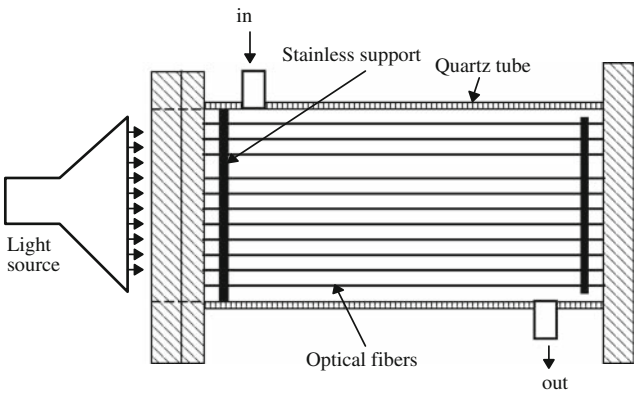

Fig. 3 Schematic of optical-fiber photoreactor

3.3 In situ FTIR on CO_2 Photoreduction

The photoreduction of CO_2 on thermal-hydrolyzed TiO_2 was studied using diffusive reflectance infrared Fourier transform (DRIFT) under UV irradiation. Zero-grade air, high-purity He and ultra-purity CO_2 (99.999 v%), from Air Products (USA) were used in the IR system. In order to reduce water interference, air and He were passed through a moisture trapper before entering the photoreactor.

A high-temperature chamber (HVC, Harrick HVC-DRP-1) made of 316 stainless steel was used as the photoreactor. There were three windows on the HVC dome. Two of them were KBr windows that were transparent to both IR and UV light for IR transmittance. The third one for UV irradiation was a quartz window that was transparent in the UV region but only partly transparent in the IR region. The photoreactor was located inside the compartment of the FTIR instrument. Pressure and gas flow rate were measured by a pressure transducer and a bubble flow meter, respectively. A *K*-type thermocouple and an electric heater were connected on the sample cup. A temperature controller, which was directly connected to the thermocouple and heater of the HVC, provided accurate temperature control (±1 °C). The HVC can be heated up to 600 °C. The UV light source (EXFO, OmniCure 1000) was supplied by a 100 W Hg lamp with filter to give light with wavelength of 365 nm only. The UV light was led to the quartz window of the HVC by an optical cable. The detailed description of the system can be found in the literature [37].

4 Results and Discussion

4.1 Photoreduction of CO_2 Using Transition-metal Loaded TiO_2

Figure 4 shows the cross-section SEM images of TiO_2, Cu/TiO_2 and Ag/TiO_2 films on top of the fibers. The TiO_2, Cu/TiO_2 and Ag/TiO_2 films are uniformly coated on the optical fiber with thicknesses of 31, 27 and 33 nm, respectively. The films appear to be transparent, colorless and flat without cracks. It is also noted from Fig. 4 that all films are consisted of very fine close-packed particles with diameters of 10–20 nm.

The XRD spectra in Fig. 5 show the diffraction patterns of TiO_2, Cu/TiO_2 and Ag/TiO_2 films. Thermal treatment at 500 °C for 5 h results in well crystallized anatase-type TiO_2. No other diffraction peak is observed in the XRD

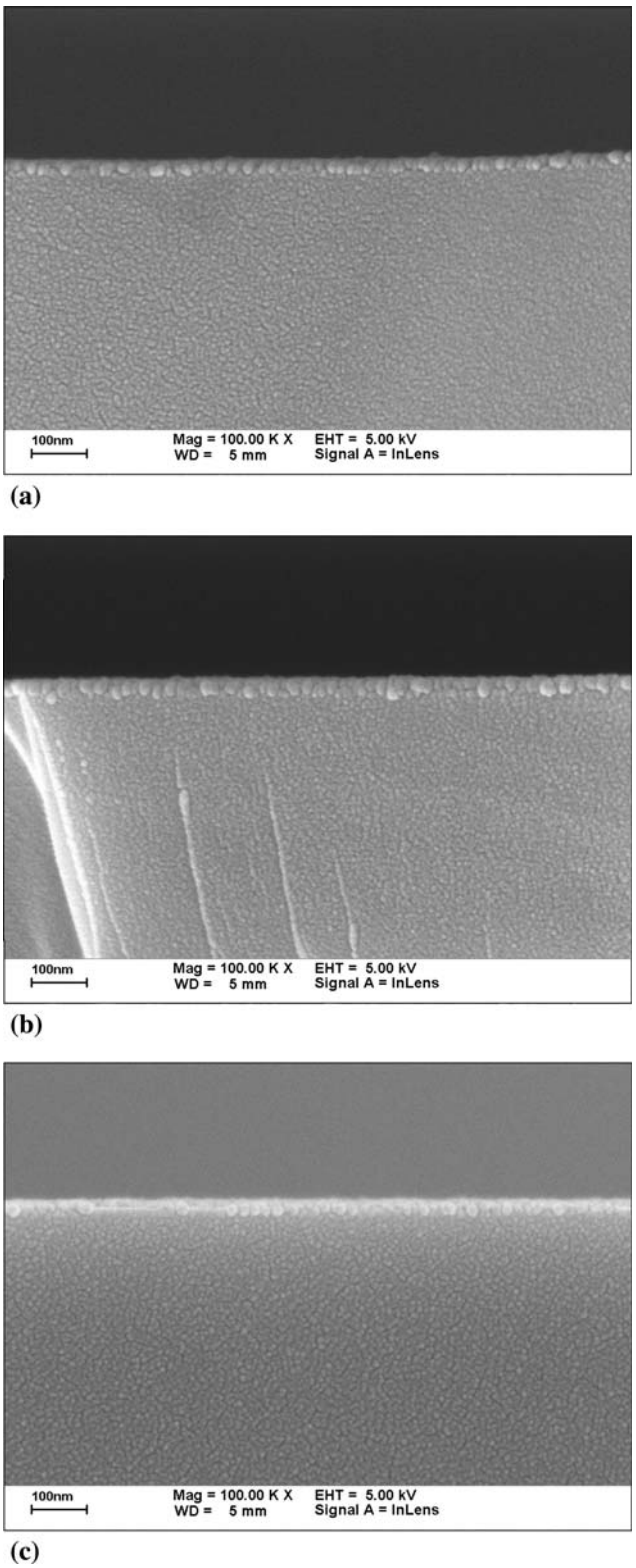

Fig. 4 Cross-section SEM images of **a** TiO_2 film, **b** Cu/TiO_2 film, **c** Ag/TiO_2 film on optical fibers

spectra indicating that metal (Cu or Ag) oxide is finely dispersed on TiO_2. Figure 6 shows the UV–visible absorption spectra of TiO_2, Cu/TiO_2 and Ag/TiO_2 films.

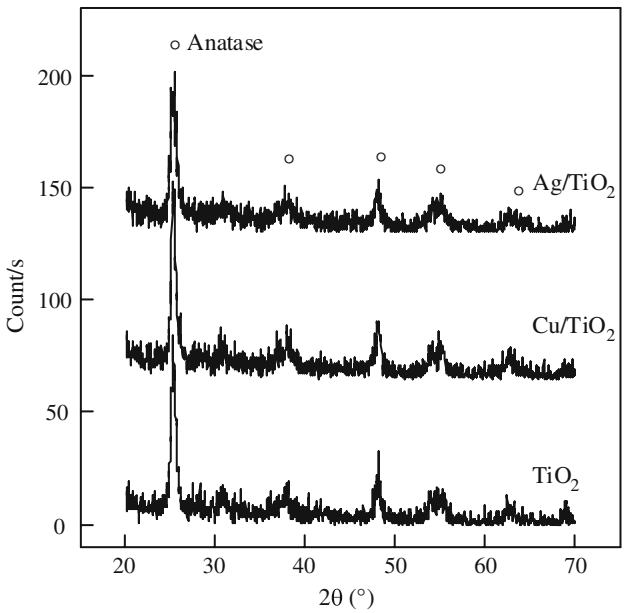

Fig. 5 XRD of TiO_2, Cu/TiO_2 and Ag/TiO_2

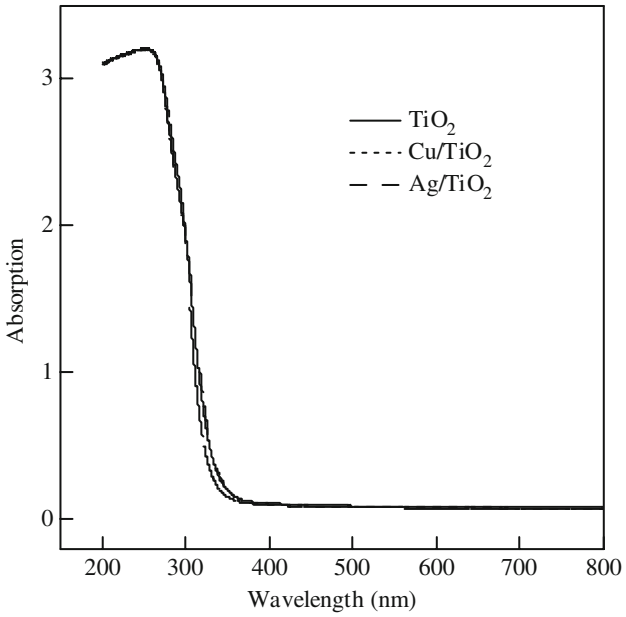

Fig. 6 UV spectra of TiO_2, Cu/TiO_2 and Ag/TiO_2

Clearly, TiO_2 film absorbs light of wavelength below 380 nm. The UV–visible absorption spectra of Cu/TiO_2 and Ag/TiO_2 photocatalysts are similar to that of pure titania.

Table 1 summarizes the characteristics of films including crystalline sizes, bandgaps and specific surface area. The average crystalline sizes of all films ranged from 14 to 17 nm, which are consistent with the SEM observation (Fig. 4). In general, the crystalline size is primarily influenced by the calcination temperature, and metal loading has negligible effect. The bandgaps ranged from 3.5 to

Table 1 Characteristics of TiO_2, Cu/TiO_2, Ag/TiO_2 films

Film	Crystal size[a] (nm)	Band gap[b] (eV)	Specific area[c] (m^2/g)
Pure TiO_2	14.4	3.6	59.8
1.2%-Cu/TiO_2	16.8	3.6	55.8
1.0%-Ag/TiO_2	12.0	3.5	71.7

[a] Calculated from the Scherrer equation according to the peak broadening of XRD spectra (at $2\theta = 25.28°$)

[b] Estimated from the UV–vis spectra extrapolating the absorption edge of UV–vis spectrum to the abscissa of zero absorption

[c] Measured by N_2 adsorption on powder samples

3.6 eV indicating that the metal loadings do not affect the band structure of TiO_2.

Figure 7 shows the methanol yield versus light intensity under the partial pressures of CO_2 and H_2O at 1.19 and 0.03 bar, respectively, at 75 °C. The yield increases with light intensity in the range of 2–10 W/cm^2. Pure TiO_2 photocatalyst gives the least methanol yield, while metal-loaded TiO_2 photocatalysts demonstrate improved yields. The activity of Cu/TiO_2 is slightly higher than that of Ag/TiO_2 when light intensity is lower than 8 W/cm^2. A maximum methanol yield of 4.12 μmole/g-cat h is obtained when 1.0 wt% Ag/TiO_2 photocatalyst was used under a light intensity of 10 W/cm^2. The light dispersion along the fibers is near the same regardless the TiO_2 layer thickness within 50–350 nm based on the wave-guide BPM [38]. Our TiO_2, Ag/TiO_2 and Cu/TiO_2 layer thicknesses are within this range. The photocatalyst layer is fully shined by

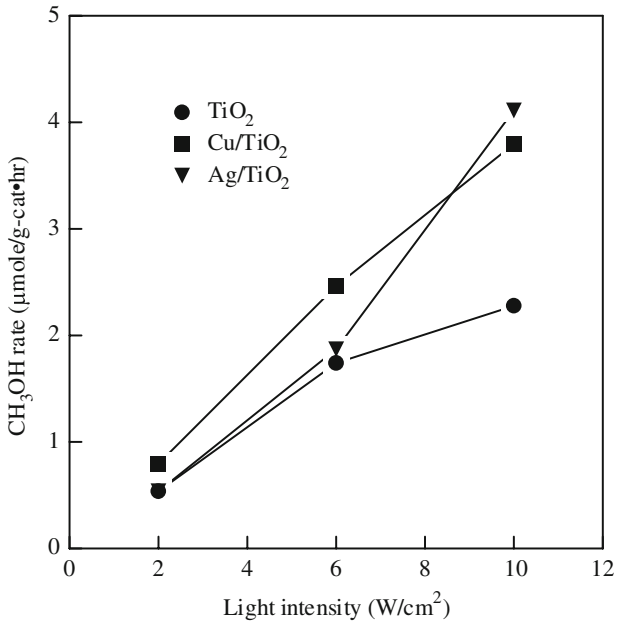

Fig. 7 Methanol yield versus light intensity on TiO_2, Cu/TiO_2 and Ag/TiO_2 (residence time = 5,000 s., $P_{CO_2} = 1.19$ bar, $P_{H_2O} = 0.03$ bar, 75 °C)

light, thus the effect of TiO_2 thickness on photo activity may be insignificant.

The heterogeneous photoreduction of CO_2 involves two steps, photo-activation and subsequent catalytic reaction, on the photocatalyst. The factors affecting photo-activation include (1) the conversion efficiency of photons to electron-hole pairs; (2) the recombination of electrons and holes; and (3) the number of effective electrons available for the photocatalytic reduction of CO_2, since large portion of the total electrons may be wasted due to migration loss. On the other hand, the factors affecting catalytic reaction include (1) the adsorption of CO_2 on the catalyst surface may be limited; (2) one of the elementary reaction steps is rate-limiting; and (3) reverse reaction of Eq. 1, i.e., oxidation of methanol, may occur.

Contact between TiO_2 and metal generally involves a redistribution of electric charge. In the presence of metal clusters, electrons are enriched owing to the alignment of Fermi levels of the metal and the semiconductor, that is, the Schottky barrier [39]. Metal, such as Cu or Ag, then serves as an electron trap that prohibits the recombination of holes and electrons. In addition, the rapid transfer of excited electrons to the Cu cluster also favors the separation of holes and electrons [40], hence significantly promotes the photoreaction.

4.2 The Influence of Mixed Oxides

$Cu–Fe/TiO_2–SiO_2$ photocatalysts were used to photo reduce CO_2 with H_2O to various kinds of products that include significant amount of ethylene and methane as well as trace amount of ethane and methanol. The optical-fiber photoreactor is maintained at 75 °C to assure that all light hydrocarbons could reach the GC detector. Consequently, no hydrocarbon product in the form of liquid was observed by naked eyes in the reactor after the photocatalytic reaction. Furthermore, owing to high redox potentials of long-chain hydrocarbons, the photoreduction of CO_2 with H_2O over $Cu–Fe/TiO_2–SiO_2$ photocatalysts to these products is impossible under UVA light and natural sunlight.

Table 2 lists the production rate of methane and ethylene over two kinds of photocatalysts under UVA. The evolution of methane is observed for two photocatalysts in which a maximum production rate of 1.860 μmol/g-cat h is measured on Cu(0.5 wt%)–Fe(0.5 wt%)/$TiO_2–SiO_2$-acac photocatalyst. Meanwhile, ethylene is only produced on photocatalysts doped with Cu and Fe metals.

Solar concentrator was employed to conduct sunlight into the reactor. The production rate of methane over $TiO_2–SiO_2$ mixed oxide photocatalysts under natural sunlight on some specific days are listed in Table 3. Methane evolution on Cu(0.5 wt%)–Fe(0.5 wt%)/$TiO_2–SiO_2$-acac photocatalyst (0.279 μmol/g-cat h) is higher than that on

bare TiO_2–SiO_2-acac counterpart (0.177 μmol/g-cat h). Since condition of natural sunlight is dependent on the weather of the day when the experiment is carried out, activities of photocatalysts towards hydrocarbon production can only be compared if the intensities of sunlight used were the same. Nevertheless, the average intensity of natural sunlight used to photo reduce CO_2 over TiO_2–SiO_2-acac photocatalyst was 6.35 mW/cm^2 on May 11, 2007 from 9.30 a.m. to 3.00 p.m. in Taipei, Taiwan. Meanwhile, photoreduction of CO_2 over Cu(0.5 wt%)–Fe(0.5 wt%)/TiO_2-SiO_2-acac photocatalyst was carried out on May 12, 2007, from 10.30 a.m. to 4.00 p.m. under an average sunlight intensity of 2.05 mW/cm^2. These results imply that the addition of Cu and Fe metals on TiO_2–SiO_2-acac photocatalyst significantly improves its photoactivity towards methane production under sunlight.

It is interestingly observed in Table 2 that TiO_2–SiO_2-acac photocatalysts are not photoactive towards ethylene production under UVA. This result could be ascribed to the much lower redox potential of methane as compared with that of ethylene [41]. When TiO_2–SiO_2 is doped with Cu and Fe metals, the resulting photocatalysts show substantial difference in hydrocarbon production as well as product selectivity. It is well known that the electrochemical reduction of CO_2 on single-crystal copper electrodes may form various kinds of hydrocarbon products depending on its index planes [42, 43]. Fe as a co-dopant on Cu/TiO_2–SiO_2 photocatalyst was observed to give rise to the synergistic performance of CO_2 reduction to ethylene.

On the other hand, only methane is produced on TiO_2–SiO_2-based photocatalysts under natural sunlight as listed in Table 3. Although Cu and Fe as dopants are observed to improve the activities of photocatalysts as indicated by the presence of significant amount of ethylene in the products under UVA, they produce only methane under natural sunlight. This result could be explained by the negligible UVA intensity in the sunlight that is filtered out by the solar concentrator. According to the manufacturer, UVA is filtered out to protect the plastic optical-fiber in the light-transmission cable against impairment. It is found in Tables 2 and 3 that bare TiO_2–SiO_2 photocatalyst only produces comparable amount of methane either under UVA with the intensity of 225 mW/cm^2 or under natural sunlight with the average intensity of 6.35 mW/cm^2. This phenomenon could infer that the increase in light intensity might be compensated by the inherent electron-hole recombination in the TiO_2–SiO_2-acac photocatalyst. On the other hand, Cu–Fe/TiO_2–SiO_2-acac in Table 3 shows strong photoactivity in methane production as compared with that of bare TiO_2–SiO_2-acac, which could be resulted from the visible-light absorption of this photocatalyst.

Table 2 Production rate of methane and ethylene over various photocatalysts under UVA

Photocatalyst[a]	Ethylene production rate (μmol/g h)[b]	Methane production rate (μmol/g h)[b]
TiO_2–SiO_2-acac	~0	0.185
Cu(0.5 wt%)–Fe(0.5 wt%)/ TiO_2–SiO_2-acac	0.211	1.860

[a] TiO_2–SiO_2 was synthesized by sol-gel process with 5 wt% of SiO_2; acac stands for the acetyl acetone as a promoter during the preparation process of TiO_2–SiO_2

[b] Methane and ethylene production rate was determined on the basis of average production rate after the reaction time of 4 h. The irradiation source was in UVA range (320–500 nm) with the intensity of 225 mW/cm^2

Table 3 Production rate of methane over TiO_2–SiO_2 mixed oxide based-photocatalysts under natural sunlight

Photocatalyst[a]	Methane production rate (μmol/g h)[b]
TiO_2–SiO_2-acac	0.177[c]
Cu(0.5 wt%)–Fe(0.5 wt%)/TiO_2–SiO_2-acac	0.279[d]

Natural sunlight was obtained by using the solar concentrator as illustrated in the Sect. 3

[a] TiO_2–SiO_2 was synthesized by sol-gel process with 5 wt% of SiO_2; acac stands for the acetyl acetone as a promoter during the preparation process of TiO_2–SiO_2

[b] Methane production rate was determined on the basis of average production rate after the reaction time of 4 h

[c] Experiment for TiO_2–SiO_2-acac photocatalyst was carried out on May 11, 2007 from 9.30 a.m. to 3.00 p.m. in Taipei, Taiwan under average solar light intensity of 6.35 mW/cm^2

[d] The experiment for Cu(0.5 wt%)–Fe(0.5 wt%)/TiO_2–SiO_2-acac was carried out on May 12, 2007, from 10.30 a.m. to 4.00 p.m. under average solar light intensity of 2.05 mW/cm^2

4.3 Dye-sensitized P25 (TiO_2) Photocatalyst

The UV–vis spectra of dye-sensitized P25 (TiO_2) thin films are shown in Fig. 8. Bare P25 inherently absorbs UV light. However, owing to the narrow bandgap of Fe_2O_3, Cu(0.5 wt%)–Fe(0.5 wt%)/P25, slight absorption in visible light is noticed as shown in Fig. 8b. When N3-dye is adsorbed on Cu(0.5 wt%)–Fe(0.5 wt%)/P25, the resulting photocatalyst depicts strong absorption in the entire visible-light region as shown in Fig. 8c. For the test of dye stability, the absorption of N3-dye–Cu(0.5 wt%)–Fe(0.5 wt%)/P25 after 6 h of photocatalytic reaction is also measured and illustrated in Fig. 8d. The UV–vis spectrum of dye-adsorbed photocatalyst after reaction is found to shift to the red region. It is well agreed that some dyes either in aqueous solution [44] or as a monolayer on Langmuir-Blodgett films [45, 46] could be aggregated under very low pH value or UV irradiation to form dimer molecules. These dimer molecules that

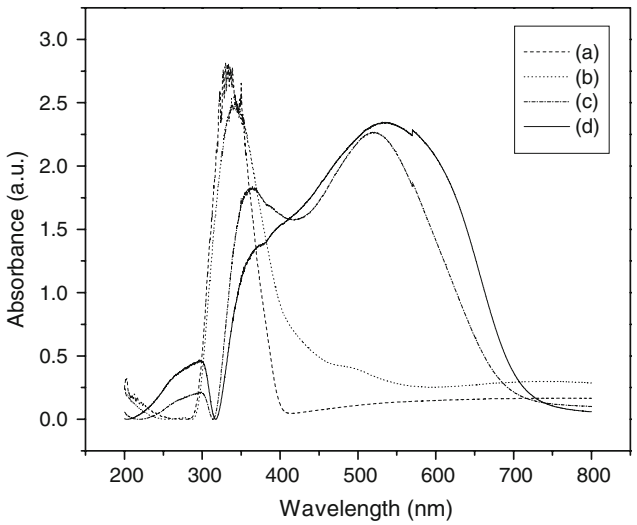

Fig. 8 UV–vis spectroscopy of different P25 (TiO_2) thin films. (*a*) P25, (*b*) Cu(0.5 wt%)–Fe(0.5 wt%)/P25, (*c*) N3-dye–Cu(0.5 wt%)–Fe(0.5 wt%)/P25-as prepared and (*d*) N3-dye–Cu(0.5 wt%)–Fe(0.5 wt%)/P25-after 6 h of reaction

are also called J-aggregate dimers were found to shift the UV–vis spectra of their corresponding monomer molecules to the red region. Accordingly, the red-shift observed in Fig. 8d could be ascribed to the above J-aggregate phenomenon. In other words, N3-dye that is adsorbed on TiO_2 photocatalyst is found to be stable under UV irradiation as well as CO_2 photoreduction. This result could be ascribed to the efficient charge transfer in N3-dye–TiO_2 system. Otherwise, N3-dye would be observed to be decomposed after the photoreaction.

The rates of methane and ethylene production over dye-sensitized Cu–Fe/P25 photocatalysts under artificial UVA light are shown in Table 4. It is found that the production rate of methane and ethylene are similar over both Cu(0.5 wt%)–Fe(0.5 wt%)/P25 and N3-dye–Cu(0.5 wt%)–Fe(0.5 wt%)/P25 photocatalysts. The results imply that N3-dye is not effective for improving the production of methane and ethylene over the photocatalyst because N3-dye absorbs mostly visible-light and covers only the surface of the photocatalyst that was coated on the optical fiber. Before the light reaches the adsorbed dye molecules, it may be scattered within the TiO_2 matrix; as a result, the capability of dye may not be fully exhibited.

The results of the experiments using concentrated natural sunlight as the irradiation source are shown in Table 5. Interestingly, N3-dye is observed to increase the methane production of Cu(0.5 wt%)–Fe(0.5 wt%)/P25 photocatalyst up to over 100%. The superior photoactivity of dye-adsorbed photocatalyst could be ascribed to the strong absorption of N3-dye in the visible-light region as presented in Fig. 8c. Although dye-adsorbed photocatalyst is observed to produce both methane and ethylene under artificial light, it is only photoactive towards methane production under concentrated natural sunlight as shown in Table 5. This result could be attributed to the UV cut-off, which might not supply enough driving force to reduce CO_2 to ethylene.

It is also interesting to compare the data in Tables 4 and 5. Under artificial light irradiation with the intensity of 225 mW/cm^2 (Table 4), the production rate of methane and ethylene over Cu(0.5 wt%)–Fe(0.5 wt%)/P25 photocatalyst are 0.575 and 0.914 μmol/g-cat h, respectively, which is found in the same order of magnitude with those of N3-dye–Cu(0.5 wt%)–Fe(0.5 wt%)/P25 counterpart. However, under the concentrated natural sunlight with the average intensity of ca. 60 mW/cm^2, Cu(0.5 wt%)–Fe(0.5 wt%)/P25 photocatalyst only produces methane with very low production rate of 0.281 μmol/g-cat h. Meanwhile, N3-dye–Cu(0.5 wt%)–Fe(0.5 wt%)/P25 photocatalyst still have the comparable methane production under concentrated natural sunlight to that under artificial light irradiation (Tables 4, 5) despite the average intensity of concentrated natural sunlight of only ca. 20 mW/cm^2. These results once again could be ascribed to the strong visible-light absorption

Table 4 Production rate of methane and ethylene over dye-sensitized P25 (TiO_2) photocatalysts under artificial light

Photocatalyst	Ethylene production rate (μmol/g-cat h)[a]	Methane production rate (μmol/g-cat h)[a]
Cu(0.5 wt%)–Fe(0.5 wt%)/P25	0.575	0.914
N3-dye–Cu(0.5 wt%)–Fe(0.5 wt%)/P25	0.562	0.847

[a] Methane and ethylene production rate were determined on the basis of average production rate after the reaction time of 4 h. The artificial light was in the range of 320–500 nm with the intensity of 225 mW/cm^2

Table 5 Production rate of methane over dye-sensitized P25 (TiO_2) photocatalysts under concentrated natural sunlight[a]

Photocatalyst	Methane production rate (μmol/g-cat h)[b]
Cu(0.5 wt%)–Fe(0.5 wt%)/P25	0.281[c]
N3-dye–Cu(0.5 wt%)–Fe(0.5 wt%)/P25	0.617[d]

[a] Concentrated natural sunlight was obtained by using the solar concentrator

[b] Methane production rate was determined on the basis of average production rate after the reaction time of 4 h

[c] Experiment for Cu(0.5 wt%)–Fe(0.5 wt%)/P25 photocatalyst was carried out in May 4, 2007 in Taipei, Taiwan from 9.20 a.m. to 2.50 p.m. under average concentrated sunlight intensity of 60 mW/cm^2

[d] Experiment for N3-dye–Cu(0.5 wt%)–Fe(0.5 wt%)/P25 photocatalyst was carried out in April 12, 2007 in Taipei, Taiwan from 9.20 a.m. to 2.50 p.m. under average concentrated sunlight intensity of 20 mW/cm^2

of the N3-dye–Cu(0.5 wt%)–Fe(0.5 wt%)/P25 photocatalyst as compared with that of Cu(0.5 wt%)–Fe(0.5 wt%)/P25 counterpart. Note that the wavelength of our artificial light is in the range of 320–500 nm while that of the concentrated sunlight is extended to the range of 500–800 nm. The N3-dye–Cu(0.5 wt%)–Fe(0.5 wt%)/P25 photocatalyst can fully absorb the light energy of 500-800 nm but Cu(0.5 wt%)–Fe(0.5 wt%)/P25 photocatalyst cannot as shown in Fig. 8. Another possible explanation for this phenomenon might be the efficient charge transfer in the N3-dye–TiO_2 system, which is supported by the stable UV–vis spectrum of the dye-adsorbed P25 after 6 h of photoreaction as illustrated in Fig. 8d.

4.4 FTIR Study on the Photocatalytic Reduction of CO_2 over TiO_2

All the IR spectra during photoreduction are subtracted by the spectrum of CO_2 adsorbed TiO_2 as background in order to clearly show the change of absorption under UV irradiation. Figure 9 shows the time-sequence IR spectra of CO_2 photoreduction over TiO_2 photocatalyst under UV irradiation in 2 h. The absorption band of bicarbonate (1,675, 1,427, 1,248 and 1,222 cm^{-1}) increased with increasing UV irradiation time. Similar trend was observed for the absorption of carbonate (1,336 cm^{-1}). One of the significant absorption bands is formic acid at 1,618 cm^{-1}, which is growing after turning on the UV light.

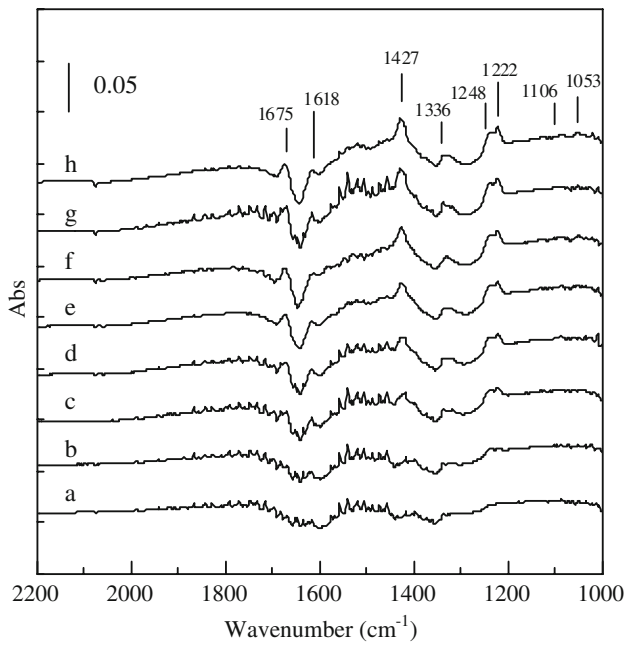

Fig. 9 IR spectra of CO_2 photoreduction over TiO_2 under UV irradiation for (*a*) 10 s, (*b*) 1 min, (*c*) 10 min, (*d*) 20 min, (*e*) 30 min, (*f*) 1 h, (*g*) 1.5 h, and (*h*) 2 h, CO_2 adsorbed TiO_2 before the UV irradiation is used as the background

Furthermore, very weak absorption bands of formaldehyde and methoxy are found at 1,106 and 1,053 cm^{-1}, respectively.

As well known in photocatalysis, electron-hole pairs are photogenerated in TiO_2 under UV irradiation to initiate a photocatalytic reaction. The mechanism of water splitting is shown in Scheme 1. Water molecule is first dissociated into H^+ and OH^- ions. Hydrogen atom is produced from H^+ by accepting an electron and adsorbed on the surface. The OH^- donates an electron to hole and becomes OH radical, which subsequently reacts with another OH radical to form H_2O_2 · H_2O_2 receives a hole to give super oxygen (O_2^-) and two H^+. One oxygen molecule is released after O_2^- donates an electron to a hole [47–50]. The O_2 generation is completed by the above procedure and released from the catalyst surface. Surface adsorbed hydrogen will be used to reduce adsorbed CO_2 to hydrocarbons in Scheme 2.

The formation of oxygen vacancies plays an important role in photocatalysis. Fujishima et al. [51] mentioned that under UV irradiation, surface oxygen atoms would be oxidized to form oxygen molecules by photogenerated holes, and then left oxygen vacancies. H_2O molecules could then be adsorbed on oxygen vacancies and split into OH groups. Oxygen vacancies or other active species, such as oxygen molecules might be photogenerated during UV irradiation.

As shown in Fig. 9, UV irradiation quickly induces the increasing of bicarbonate (1,675, 1,427 cm^{-1}) and carbonate (1,336 cm^{-1}). The photogenerated OH group and oxygen vacancy further increase the amount of bicarbonate and carbonate which are converted from gas-phase CO_2. However, once bicarbonate or carbonate is formed, it will become

$$TiO_2 \xrightarrow{h\upsilon} e^- + h^+$$

$$H_2O \rightarrow H^+ + OH^-$$

$$H^+ + e^- \rightarrow H \rightarrow \begin{array}{c} H \\ | \\ TiO_2 \end{array} \text{ or } \begin{array}{c} H \\ | \\ Cu \end{array}$$

$$OH^- + h^+ \rightarrow OH\bullet$$

$$2OH\bullet \rightarrow H_2O_2$$

$$H_2O_2 + h^+ \rightarrow O_2^- + 2H^+$$

$$O_2^- + h^+ \rightarrow O_2$$

Scheme 1 Surface photoreaction of H_2O splitting

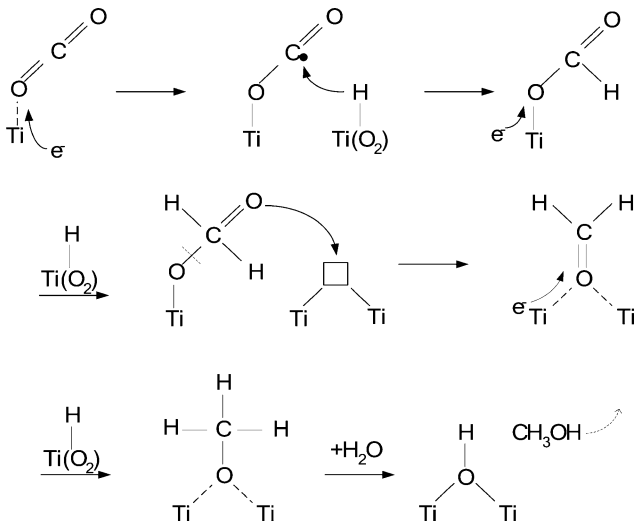

Scheme 2 Proposed mechanism of photocatalytic CO_2 reduction over TiO_2

very stable on the TiO_2 surface and no further conversion is possible.

Formic acid (1,618 cm^{-1}), formaldehyde (1,106 cm^{-1}) and methoxy (1,053 cm^{-1}) emerge and increase after UV irradiation as shown in Fig. 9. Obviously these species are produced from the photoreduction of adsorbed CO_2. They are the intermediates in the elementary steps of CO_2 photoreduction over TiO_2. Other possible intermediates may also exist but cannot be detected due to the detection limitation of IR measurement.

Scheme 2 illustrates the mechanism of adsorbed CO_2 which is further photocatalytically reduced to hydrocarbons under UV irradiation. Starting from the adsorbed linear CO_2, format (HCOO) is formed by accepting an electron and adding one hydrogen atom. Dioxymethylene (H_2COO) is formed from the format by adding one hydrogen atom, and then migrates to the adjacent oxygen vacancy to form formaldehyde (H_2CO) by accepting one electron. In this step, one oxygen is detached from dioxymethylene and left on the previous TiO_2 site. Methoxy (CH_3O) is then formed by adding another hydrogen atom. Finally, methoxy reacts with free surface H_2O and converts to methanol, and then leaves one OH group on TiO_2 surface after methanol is desorbed from the surface.

The reduction of CO_2 to methanol requires reducing the chemical state of carbon from C (4+) to C (2−). Six electrons are required for each methanol. Overall, considering Schemes 1 and 2, three hydrogen atoms and three electrons progressively transfer to one adsorbed CO_2 resulting in the formation of one methoxy. Methoxy with one water molecule eventually converts to methanol. Six holes acquire the electrons step by step from OH^- and H_2O_2 resulting in the production of 1.5 O_2 as shown in Scheme 1. In summary, two H_2O are consumed.

5 Conclusion

An optical-fiber photoreactor has been designed and applied to the photoreduction of CO_2 with H_2O using TiO_2, Cu/TiO_2, Ag/TiO_2, $Cu–Fe/TiO_2–SiO_2$ and dye-sensitized Cu–Fe/P25 coated optical fibers. The photoreduction of CO_2 is one of the best routes to realize renewable energy similar to photosynthesis. Compared with a traditional packed-bed reactor, an optical fiber provides a medium to transmit light uniformly throughout a reactor. In addition, a higher processing capacity is possible because the photocatalyst can be disperse on the optical fibers with large surface area in a given reactor volume. The advantage of photo-driven reaction is clearly benefited from the unlimited solar energy. However, further improvement in the photocatalytic reduction of CO_2 is still needed.

References

1. Laws EA, Berning JL (1991) Bioresour Technol 37:25
2. Yamashita H, Fujii Y, Ichihashi Y, Zhang SG, Ikeue K, Park DR, Koyano K, Tatsumi T, Anpo M (1998) Catal Today 45:221
3. Anpo M, Yamashita H, Ichihashi Y, Ehara S (1995) J Electroanal Chem 396:21
4. Pathak P, Meziani MJ, Li Y, Cureton LT, Sun YP (2004) Chem Commun 10:1234
5. Tseng IH, Chang W-C, Wu JCS (2002) Appl Catal B: Environm 37:37
6. Lo CC, Hung CH, Yuan CS, Wu JF (2007) Sol Energy Mater Sol Cells 91:1765
7. Dey GR, Belapurkar AD, Kishore K (2004) J Photochem Photobiol A: Chem 163:503
8. Guan GQ, Kida T, Harada T, Isayama M, Yoshida A (2003) Appl Catal A: Gen 249:11
9. Guan GQ, Kida T, Yoshida A (2003) Appl Catal B: Environm 41:387
10. Yahaya AH, Gondal MA, Hameed A (2004) Chem Phys Lett 400:206
11. Chen H-C, Chou H-C, Wu JCS, Lin H-Y (2008) J Mater Res 23:1364
12. Pan PW, Chen YW (2007) Catal Commun 8:1546
13. Ozcan O, Yukruk F, Akkaya EU, Uner D (2007) Appl Catal B: Environm 71:291
14. Ozcan O, Yukruk F, Akkaya EU, Uner D (2007) Top Catal 44:523
15. Nguyen T-V, Wu JCS, Chiou C-H (2008) Catal Commun 9:2073
16. Hirose T, Maeno Y, Himeda Y (2003) JMol Catal A-Chem 193:27
17. Pathak P, Meziani MJ, Castillo L, Sun YP (2005) Green Chem 7:667
18. Sasirekha N, Basha SJS, Shanthi K (2006) Appl Catal B: Environm 62:169
19. Zhao ZH, Fan JM, Wang ZZ (2007) J Clean Prod 15:1894
20. Hofstadler K, Bauer R, Novalic S, Heisler G (1994) Environ Sci Technol 28:670
21. Danion A, Bordes C, Disdier J, Gauvrit JY, Guillard C, Lanteri P, Jaffrezic-Renault N (2004) J Photochem Photobiol A: Chem 168:161
22. Danion A, Disdier J, Guillard C, Abdelmalek F, Jaffrezic-Renault N (2004) Appl Catal B: Environm 52:213

23. Danion A, Disdier J, Guillard C, Abdelmalek F, Jaffrezic-Renault N (2006) Int J Appl Electrom 23:187
24. Danion A, Disdier J, Guillard C, Jaffrezic-Renault N (2007) J Photochem Photobiol A: Chem 190:135
25. Danion A, Disdier J, Guillard C, Paisse O, Jaffrezic-Renault N (2006) Appl Catal B: Environm 62:274
26. Peill NJ, Bourne L, Hoffmann MR (1997) J Photochem Photobiol A: Chem 108:221
27. Peill NJ, Hoffmann MR (1995) Environ Sci Technol 29:2974
28. Peill NJ, Hoffmann MR (1996) Environ Sci Technol 30:2806
29. Peill NJ, Hoffmann MR (1997) J Energ-T Asme 119:229
30. Peill NJ, Hoffmann MR (1998) Environ Sci Technol 32:398
31. Xu JJ, Ao YH, Fu DG, Lin J, Lin YH, Shen XW, Yuan CW, Yin ZD (2008) J Photochem Photobiol A: Chem 199:165
32. Chu T, Huang H, Tsai D (2006) Annual meeting of physics. American Physical Society, Taipei
33. Wu JCS, Lin HM, Lai CL (2005) Appl Catal A: Gen 296:194
34. Lo CF, Wu JCS (2005) J Chin Inst Chem Eng 36:119
35. Nguyen TV, Choi DJ, Yang OB (2005) Res Chem Intermed 31:483
36. Nguyen TV, Lee HC, Yang OB (2006) Sol Energy Mater Sol Cells 90:967
37. Wu JCS, Cheng Y-T (2006) J Catal 237:393
38. Wu J, Wu T-H, Chu T, Huang H, Tsai D (2008) Top Catal 47:131
39. Linsebigler AL, Lu GQ, Yates JT (1995) Chem Rev 95:735
40. Hirano K, Inoue K, Yatsu T (1992) J Photochem Photobiol A: Chem 64:255
41. Gattrell M, Gupta N, Co A (2006) J Electroanal Chem 594:1
42. Hori Y, Takahashi I, Koga O, Hoshi N (2002) J Phys Chem B 106:15
43. Hori Y, Wakebe H, Tsukamoto T, Koga O (1995) Surf Sci 335:258
44. Habibi MH, Hassanzadeh A, Zeini-Isfahani A (2006) Dyes Pigments 69:111
45. Tachibana H, Yamanaka Y, Sakai H, Abe M, Matsumoto M (2000) J Lumin 87–9:800
46. Kuroda S (2004) Adv Colloid Interface Sci 111:181
47. Anpo M, Aikawa N, Kubokawa Y (1984) J Phys Chem 88:3998
48. Inoue T, Fujishima A, Konishi S, Honda K (1979) Nature 277:637
49. Howe RF, Gratzel M (1987) J Phys Chem 91:3906
50. Serpone N, Lawless D, Disdier J, Herrmann J-M (1994) Langmuir 10:643
51. Fujishima A, Rao TN, Tryk DA (2000) J Photochem Photobiol C: Rev 1:1